Automatic Measurement of the Dependence on Pressure and Temperature of the Mass Density of Drilling Fluids

E. Cayeux[1]*

[1]Norwegian Research Center

Summary

Drilling fluids are subject to substantial variations in pressure and temperature while they are circulated in a well. These changes are so great that the mass density of the drilling fluid varies significantly during circulation. Accurate estimation of the hydrostatic and hydrodynamic pressures therefore requires a reliable model of the pressure and temperature dependence of the mass density of the drilling fluid. Usually, the mass density of a drilling fluid is measured manually with a mud balance. The pressure and temperature dependence of the mass density of the fluid [i.e., its pressure, volume, and temperature (PVT) behavior] is then calculated from a PVT model of its components and their relative proportions. However, variations in the composition of the fluid mix and uncertainties in the PVT behavior of each component may lead to inaccuracies. To overcome these limitations, an apparatus has been designed to measure the PVT behavior of the drilling fluid directly and automatically. The setup measures both the mass density and the speed of sound of the fluid at specific conditions of pressure and temperature. It is possible to estimate the adiabatic compressibility from the speed of sound in the liquid mix. The device utilizes a heat exchanger from which the specific heat capacity of the drilling fluid can be derived. The isothermal compressibility can be calculated by combining the specific heat capacity and the adiabatic compressibility. While estimating the specific heat capacity using the heat exchanger, the thermal conductivity of the fluid is also estimated as a byproduct. A PVT model of the drilling fluid is obtained by combining measurements made at different conditions of pressure and temperature. The automatic and continuous provision of drilling fluid PVT behavior enhances the precision of model predictive drilling control systems and, at the same time, can simplify their configuration, therefore making them more accessible to any drilling operation.

Introduction

Drilling fluid mass density is essential for the calculation of the hydrostatic pressure in a borehole. It is also an important parameter in viscous friction calculations because it appears in the Navier-Stokes equation and in buoyancy calculations when performing torque and drag or drillstring dynamic analysis. During drilling operations, the drilling fluid mass density is usually measured with a mud balance at regular intervals. The precision of the mud balance measurements is about ±10 kg/m^3. Furthermore, drilling fluids are subject to a wide range of pressures and temperatures, and therefore the drilling fluid mass density cannot be assumed to be constant for the range of depths of normal oilfield wells. Isambourg et al. (1996) found that the pressure and temperature dependence of drilling fluids can be described by a biquadratic function in the temperature range of 20–200°C and a range of pressure between 1 and 1400 bar. The biquadratic model proposed by Isambourg has since been used in a more recent study (Hermoso et al. 2017). Based on multiple published density measurements made on various fluids (Zamora et al. 2000, 2012; McMordie et al. 1982; Peters et al. 1990; Hemphill and Isambourg 2005; Demirdal and Cunha 2007, 2009; Demirdal et al. 2007; Hussein and Amin 2010), it has been found that the PVT model can be reduced to a linear function of temperature combined with a quadratic form of pressure without losing much of its accuracy and which is the model published in *API RP 13D* (2017):

$$\rho_m = \left(A_m + B_m T\right) + \left(C_m + D_m T\right) p + \left(E_m + F_m T\right) p^2, \quad (1)$$

where ρ_m is the mass density, T is the temperature, p is the pressure, and A_m, B_m, C_m, D_m, E_m, and F_m are the parameters of the PVT model. The accuracy of the model described by Eq. 1 is about 0.35% on average with a standard deviation of 0.23% for a temperature range from 3 to 260°C and pressures from 1 to 2000 bar, based on measurements of 26 different fluids.

Calibrating Eq. 1 for a particular drilling fluid requires access to a high-pressure and -temperature densitometer, which is not routinely available at the rigsite, except, perhaps, during drilling operations in high-pressure, high-temperature conditions. The alternative is to estimate the parameters of the PVT model by combining the PVT behavior of each component of the drilling fluid. Because a drilling fluid is a mixture of solids and liquids, its mass density is simply the volumetric weighted average of all the components:

$$\rho_m = \sum_{i \in \Omega} f_i \rho_i, \text{ with } \sum_{i \in \Omega} f_i = 1, \quad (2)$$

where ρ_m is the drilling fluid mass density, Ω is the set of indices for the different components, f_i is the volume fraction of the ith component, and ρ_i is its corresponding mass density.

*Corresponding author; email: eric.cayeux@norceresearch.no

This paper (SPE 204084) was accepted for presentation at the SPE/IADC International Drilling Conference and Exhibition, Virtual, 8–12 March 2021, and revised for publication. Original manuscript received for review 25 April 2022. Revised manuscript received for review 20 June 2022. Paper peer approved 13 July 2022.

The PVT behavior of several aqueous solutions of NaCl, NaBr, KCl, KBr, $CaCl_2$, $CaBr_2$, $ZnCl_2$, and $ZnBr_2$ has been described by Kemp et al. (1989). Their model is relatively complex and does not reduce to Eq. 1. For that reason, Eq. 1 has been expanded to account for the concentration of salt by replacing the parameter A_o with a cubic form of the weight of salt:

$$\rho_w = \left(S_0 + S_1 w_t + S_2 w_t^2 + S_3 w_t^3 + B_w T\right) + \left(C_w + D_w T\right) p + \left(E_w + F_w T\right) p^2, \quad (3)$$

where ρ_w is the mass density of the brine and w_t is the weight fraction of the salt at the normal condition of temperature and pressure (atmospheric pressure and 297 K). S_0, S_1, S_2, S_3, B_w, C_w, D_w, E_w, and F_w are the coefficients of the model as published in *API RP 13D* (2017).

The PVT behavior of base oils can also be described by Eq. 1. Zamora et al. (2013) presented parameters for several base oils and some brines. Moreover, the solid components have coefficients of thermal expansion and compressibility (Isambourg et al. 1996) which should be accounted for. Knowing the PVT characteristics of each component, it is possible to estimate the mass density of the fluid mixture with Eq. 2. However, as the various components have different compressibilities and thermal expansion characteristics, the volumetric fraction of each component changes with pressure and temperature. A method to calculate changes in volume fractions with pressure and temperature is described by Cayeux et al. (2014).

In practice, the downhole drilling fluid density will also be influenced by the presence of cuttings, dissolution of formation solids, absorption of formation fluids in the liquid phase, and barite sagging. These additional considerations are not addressed in this paper because the objective is to propose an alternative system of surface measurement to those which are, themselves, subject to the same limitations.

However, the problem remains that the composition of the drilling fluid changes continuously throughout a drilling operation, either because of the actions taken by the fluid engineer to maintain the quality of the drilling fluid or because formation fluids and solids are entrained during circulation. Even more problematically, it is often not easy to get an accurate description of the component quantities of the drilling fluid. Cayeux (2020) illustrated the impact of this lack of information on the estimated hydrostatic pressure. For instance, if the drilling fluid density is known at atmospheric pressure and 50°C (e.g., 1700 kg/m^3) and nothing else, the 95 percentile estimate of the hydrostatic pressure at 3500 mTVD (true vertical depth), lies between −5 and +7 bar **(Fig. 1a).** However, for an oil-based fluid (OBM) with a 70/30 oil/water ratio (OWR), the 95 percentile at 3500 mTVD reduces to −2.5 and +3 bar **(Fig. 1b)**. Knowing the fluid density for a water-based drilling fluid (WBM) at three different temperatures under atmospheric conditions will reduce the confidence interval, but only to −4 to 5.5 bar **(Fig. 1c)**.

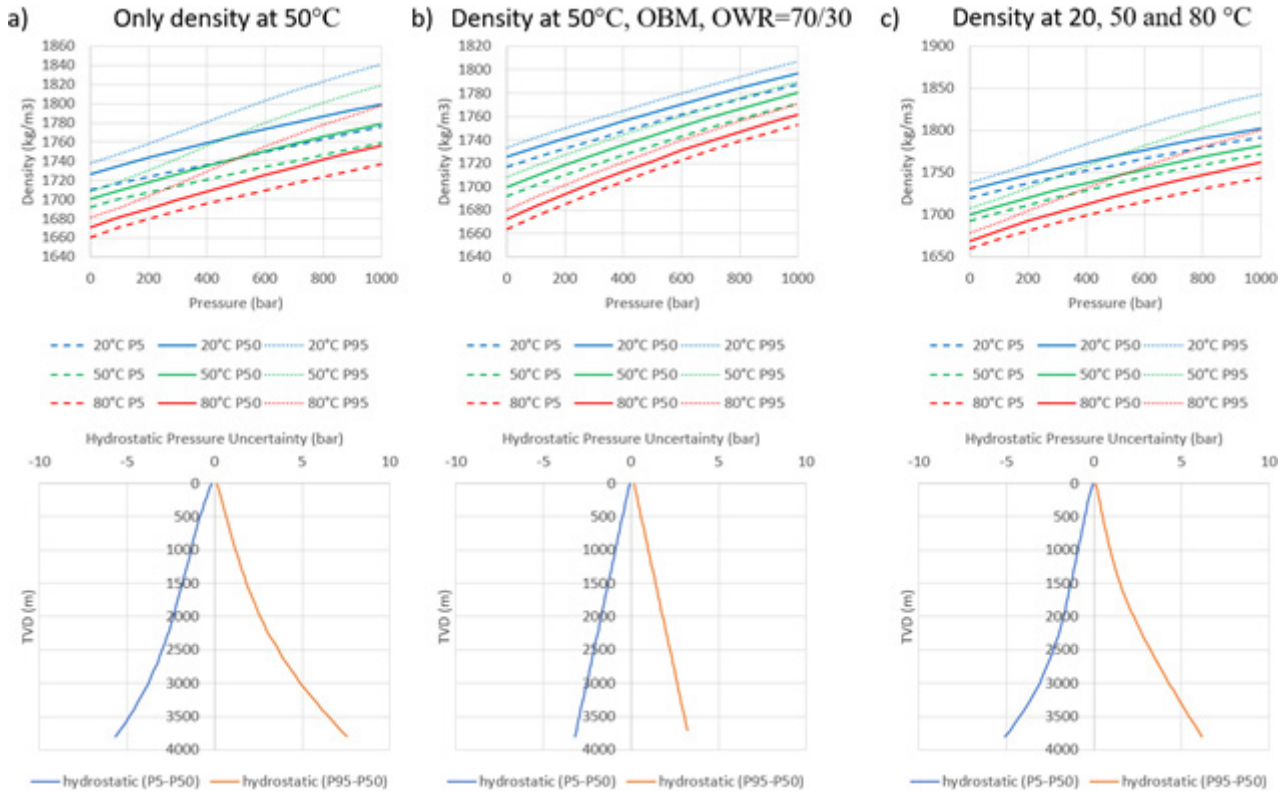

Fig. 1—(a) Impact of an unspecified drilling fluid of mass density 1700 kg/m^3 on the estimated hydrostatic pressure. (b) Hydrostatic pressure variations based on the additional knowledge that the fluid is an OBM with an OWR of 70/30. (c) Impact on hydrostatic pressure estimates for a WBM with mass density measurements at three different temperatures under atmospheric conditions (Cayeux 2020).

Having to rely on manual measurements and assumptions about the drilling fluid formulation presents difficulties when trying to automate the drilling process. Therefore, it would be a considerable advantage if the drilling fluid mass density could be measured in real time. Although such information is available on some rigs, it would be even better to obtain a full description of the drilling fluid PVT characteristics directly from inline measurements. Therefore, the goal of the present work is to establish whether it is possible to design an inline apparatus capable of measuring the PVT behavior of a drilling fluid with acceptable precision (for example, to ±5%) over a wide range of pressures and temperatures, typically 10–200°C and from 1 to 2000 bar.

Inline PVT Measurement

Because Eq. 1 has six parameters, it is necessary to have at least six measurements made under different conditions of pressure and temperature. An obvious approach would be to measure the mass density of the fluid under six different pairs of pressure and temperature; consequently, from Eq. 1, the following set of simultaneous equations can be written:

$$\begin{cases} \rho_{m_1} = (A_m + B_m T_1) + (C_m + D_m T_1) p_1 + (E_m + F_m T_1) p_1^2 \\ \rho_{m_2} = (A_m + B_m T_2) + (C_m + D_m T_2) p_2 + (E_m + F_m T_2) p_2^2 \\ \rho_{m_3} = (A_m + B_m T_3) + (C_m + D_m T_3) p_3 + (E_m + F_m T_3) p_3^2 \\ \rho_{m_4} = (A_m + B_m T_4) + (C_m + D_m T_4) p_4 + (E_m + F_m T_4) p_4^2 \\ \rho_{m_5} = (A_m + B_m T_5) + (C_m + D_m T_5) p_5 + (E_m + F_m T_5) p_5^2 \\ \rho_{m_6} = (A_m + B_m T_6) + (C_m + D_m T_6) p_6 + (E_m + F_m T_6) p_6^2 \end{cases}, \quad (4)$$

where ρ_{m1}, ρ_{m2}, ρ_{m3}, ρ_{m4}, ρ_{m5}, and ρ_{m6} are the measured mass densities at the respective conditions of pressure and temperatures (p_1, T_1), (p_2, T_2), (p_3, T_3), (p_4, T_4), (p_5, T_5), and (p_6, T_6). This system of equations is linear in A_m, B_m, C_m, D_m, E_m, and F_m and can be easily solved using a Gauss-Jordan method, for instance (Teukolsky et al. 1992).

It is desirable to avoid operating at high pressures and temperatures to keep the design of the apparatus as simple as possible. Considering that the model of Eq. 1 has an average accuracy of about 0.35% over a range of temperatures spanning more than 250°C and a range of pressures up to 2000 bar, it is possible to calibrate the parameters with measurements made on a smaller range of pressures and temperatures. However, the accuracy of the calibrated model will depend on the accuracy of measurements and the range of pressures and temperatures over which they are taken. **Fig. 2** illustrates how measurement uncertainty and the associated range of measurements influence the uncertainty of the extrapolated value when utilizing a model of known precision. In this illustration, the model is calibrated using randomly chosen values of the measurements within their accuracy range to provide a stochastic description of the envelope of model predictions outside the measurement range. The precision of the measurements limits the acceptable extrapolation range, and a narrow measurement range results in increasing uncertainties the greater the extrapolation.

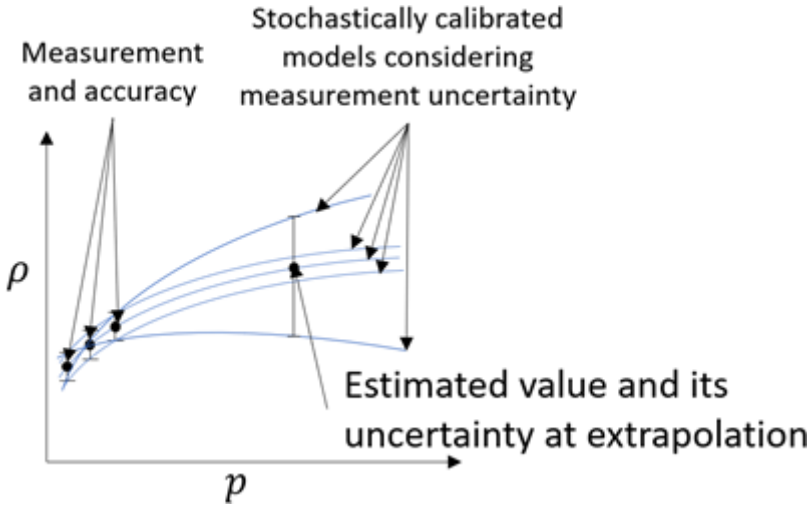

Fig. 2—Illustration of the impact of measurement accuracy and domain span on the uncertainty of the extrapolated value.

Accounting for model accuracy and measurement precision and repeatability, it is useful to establish a calibration range of pressures and temperatures for the sample measurements that will permit extrapolation of the model to higher pressures and temperatures with acceptable accuracy. If the densitometer has a measurement precision of 0.05 kg/m^3 and repeatability of 0.01 kg/m^3, based, for example, on an Anton Paar L-dens 7500 inline densitometer, stochastic simulations can be run to quantify the measurement error for a suitable calibration range of pressures and temperatures. Measurement precision is regarded as a source of systematic error (i.e., one randomly drawn value is applied to all measurements), while measurement repeatability is considered as a random error drawn individually for each measurement. For example, if the PVT model is to be used over a range of 1000 bar and 200°C, the root mean square (RMS) of the difference between the predicted density and the "true" value can be calculated with random variations in the systematic bias of the density measurement when the calibration samples lie within a small range of pressure and temperature. The results of 250 stochastic simulations presented in **Fig. 3** show that to achieve a 5% average accuracy for the entire range of 1000 bar and 200°C, it is necessary to use a calibration range of at least 30 bar and 25°C.

A possible design for an inline apparatus could involve pumping the drilling fluid past a controllable heating element with a controllable choke downstream of a densitometer applying backpressure while measuring the mass density **(Fig. 4).** The set points for the heating element and the choke could be changed six times to collect the necessary mass densities to calibrate the PVT model of Eq. 1. However, in practice, the measurement sequence would take too long because changing the heating element temperature would require time to equilibrate. Gathering a complete set of calibration measurements might easily take 15–30 minutes. In practice, with a typical annular velocity of 0.8 m/s, if PVT measurements are available every 30 minutes, then the same measured values would apply for an annular fluid column of about 1400 m in length. In a typical deep well, it might mean only four or five PVT measurements in the entire annulus. This would affect the resolution of the bottomhole pressure estimate, especially if the device had measured a momentarily heavy or light sample from the mud system. Conversely, if the PVT measurements are available every 30–60 seconds, with typical annular velocities around

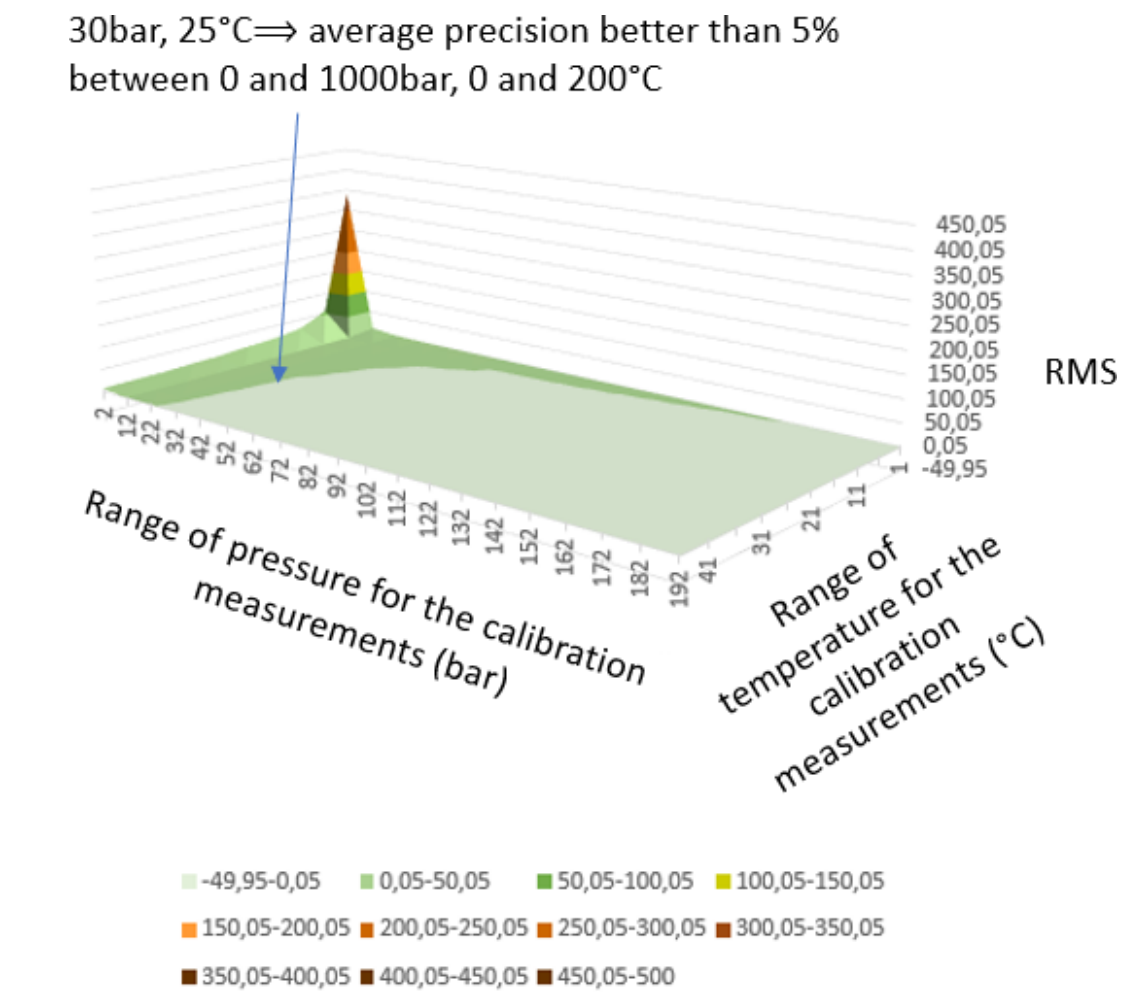

Fig. 3—RMS value of an extrapolated PVT model for a range of pressures spanning 1000 bar and a range of temperatures of 200°C, when the calibration measurements are taken within a range of temperatures given on the *x*-axis and a range of pressures given in the *y*-axis. The results are based on a densitometer having a measurement accuracy of 0.05 kg/m^3 and 250 stochastic simulations.

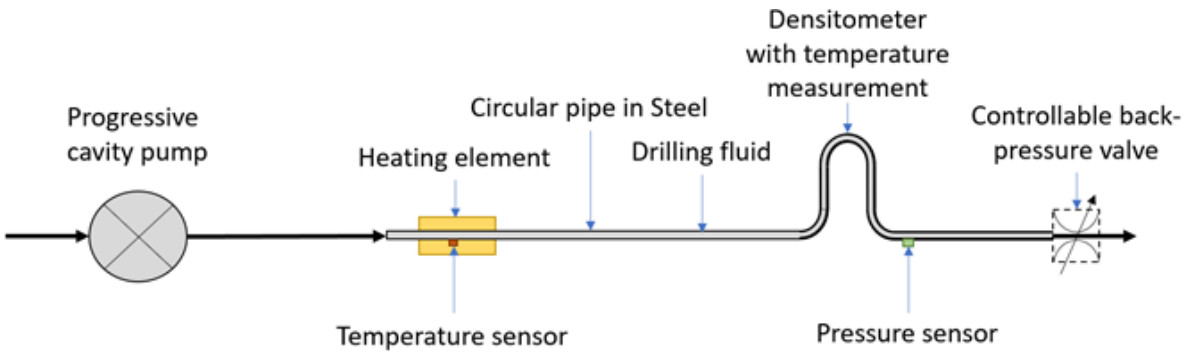

Fig. 4—Possible design of a PVT inline setup where various temperature and pressure conditions can be applied to a drilling fluid to collect at least six measurements of mass density under variable conditions of pressures and temperatures.

0.8–1 m/s, the same PVT measurement will apply for about 30 m (i.e., one stand), which is a reasonable discretization length for hydraulic calculations. So, the aim of the inline PVT measurement device should be to provide measurements at most every minute.

To speed up measurements, an alternative would be to perform six measurements simultaneously. **Fig. 5** shows a configuration where the densitometers are mounted in series. The configuration would consist of six parallel branches or any combination of series and parallel branches. **Fig. 6** depicts two parallel branches where, in one branch, the temperature of the fluid remains constant, while in the second, it is changed. For each of the branches, backpressure is applied at two intermediate positions. This configuration has the advantage of fewer chokes and pressure sensors, four instead of five.

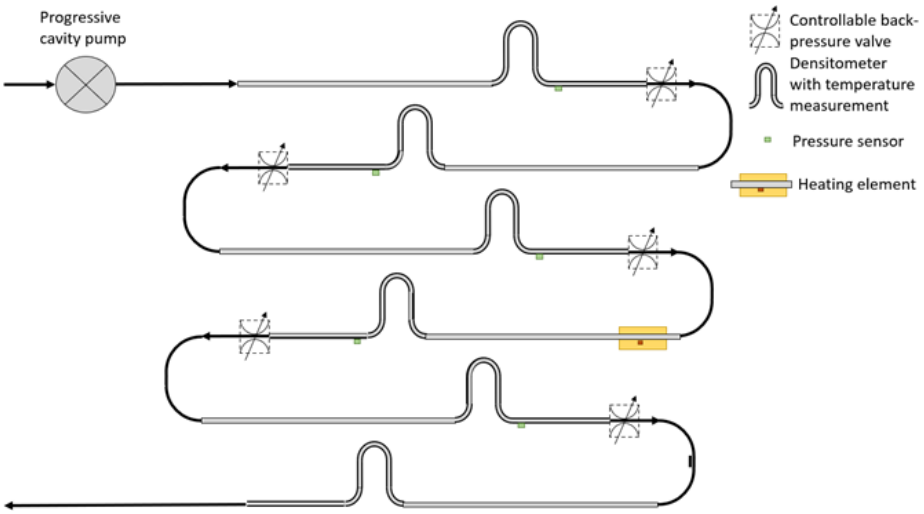

Fig. 5—Simultaneous measurements of mass density under six conditions of pressures and temperatures. Here, the densitometers are configured in series.

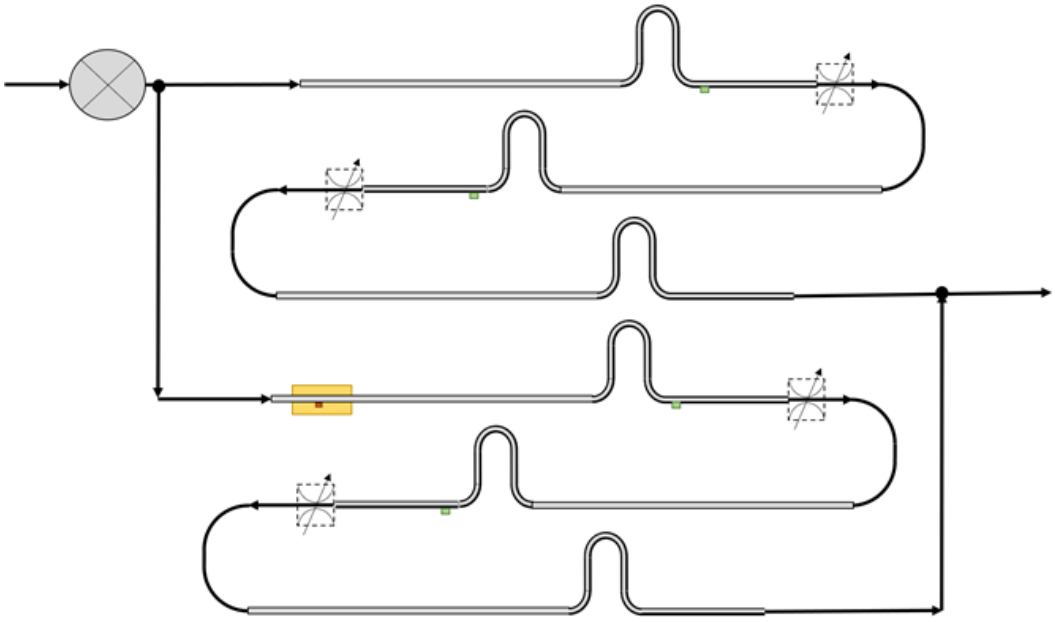

Fig. 6—Simultaneous measurements of mass density under six conditions of pressures and temperatures. Here, in a combined parallel and series configuration.

With simultaneous measurements of mass density, it is possible to provide in real time a complete, calibrated, PVT model. Yet, the circuitry is complex, involving four or five chokes. Therefore, it would be worthwhile to investigate whether the hydraulic circuit could be further simplified.

Reducing the Number of Pressure and Temperature Conditions

The pressure and temperature dependence of drilling fluid densities is related to the fluid compressibility and its thermal dilatation. Therefore, if it is possible to directly measure the fluid compressibility, it would be possible to simplify the setup and reduce the number of pressure and temperature conditions required for the solution. The isothermal compressibility (κ_T) of a fluid is defined as follows (Landau and Lifshitz 1980):

$$\kappa_T = -\frac{1}{V}\left(\frac{\partial V}{\partial p}\right)_T, \quad (5)$$

where V is the volume that is related to the mass density through

$$V = \frac{m}{\rho_m}, \quad (6)$$

where m is the mass of matter contained in the volume V. It is possible to express the isothermal compressibility of the fluid in terms of the PVT model described in Eq. 1:

$$\kappa_T = \frac{\left(C_m + D_m T\right) + 2\left(E_m + F_m T\right) p}{\left(A_m + B_m T\right) + \left(C_m + D_m T\right) p + \left(E_m + F_m T\right) p^2} = \frac{1}{\rho_m}\left(\left(C_m + D_m T\right) + 2\left(E_m + F_m T\right) p\right). \tag{7}$$

Let us now consider the definition of the speed of sound (c) in matter:

$$c^2 = \left(\frac{\partial p}{\partial \rho}\right)_S, \tag{8}$$

where S is the entropy. Then, the isentropic compressibility is defined as follows:

$$\kappa_S = -\frac{1}{V}\left(\frac{\partial V}{\partial p}\right)_S, \tag{9}$$

and it is possible to express a relation between the isentropic compressibility to the speed of sound in the medium:

$$\kappa_S = \frac{1}{\rho c^2}. \tag{10}$$

Finally, the isentropic compressibility is related to the isothermal compressibility through the following relation (Landau and Lifshitz 1980):

$$\kappa_S = \kappa_T - \frac{\alpha^2 T}{\rho C_p}, \tag{11}$$

where $\alpha = \frac{1}{V}\left(\frac{\partial V}{\partial T}\right)_p$ is the volumetric coefficient of thermal expansion and C_p is the isobaric specific heat capacity. It is possible to express the volumetric coefficient of thermal expansion in terms of the PVT model described in Eq. 1:

$$\alpha = -\frac{B_m + D_m p + F_m p^2}{\left(A_m + B_m T\right) + \left(C_m + D_m T\right) p + \left(E_m + F_m T\right) p^2} = -\frac{1}{\rho_m}\left(B_m + D_m p + F_m p^2\right). \tag{12}$$

Thus, if the mass density and the speed of sound are measured at the same time, six equations can be obtained with only three combinations of pressure and temperature:

$$\begin{cases} \frac{1}{c_1^2} = \left(\left(C_m + D_m T_1\right) + 2\left(E_m + F_m T_1\right) p_1\right) - \frac{T_1}{\rho_{m_1}^2 C_{p_{T_1}}}\left(B_m + D_m p_1 + F_m p_1^2\right)^2 \\ \frac{1}{c_2^2} = \left(\left(C_m + D_m T_2\right) + 2\left(E_m + F_m T_2\right) p_2\right) - \frac{T_2}{\rho_{m_2}^2 C_{p_{T_2}}}\left(B_m + D_m p_2 + F_m p_2^2\right)^2 \\ \frac{1}{c_3^2} = \left(\left(C_m + D_m T_3\right) + 2\left(E_m + F_m T_3\right) p_3\right) - \frac{T_1}{\rho_{m_3}^2 C_{p_{T_3}}}\left(B_m + D_m p_3 + F_m p_3^2\right)^2 \\ \rho_{m_1} = \left(A_m + B_m T_1\right) + \left(C_m + D_m T_1\right) p_1 + \left(E_m + F_m T_1\right) p_1^2 \\ \rho_{m_2} = \left(A_m + B_m T_2\right) + \left(C_m + D_m T_2\right) p_2 + \left(E_m + F_m T_2\right) p_2^2 \\ \rho_{m_3} = \left(A_m + B_m T_3\right) + \left(C_m + D_m T_3\right) p_3 + \left(E_m + F_m T_3\right) p_3^2 \end{cases}, \tag{13}$$

where c_1, c_2, and c_3 are the respective speeds of sound for the conditions of pressure and temperature (p_1, T_1), (p_2, T_2), and (p_3, T_3), κ_{p_1,T_1}, κ_{p_2,T_2}, and κ_{p_3,T_3} are the estimated isothermal compressibility coefficients at the respective conditions of pressure and temperature (p_1, T_1), (p_2, T_2), and (p_3, T_3), and α_{p_1,T_1}, α_{p_2,T_2}, and α_{p_3,T_3} are the estimated volumetric coefficients of thermal expansion at the respective conditions of pressure and temperature (p_1, T_1), (p_2, T_2), (p_3, T_3).

The resulting system of equations is nonlinear. To solve that system of equations, Eq. 13 is reformulated:

$$Ax - BX_1 x - CX_2 x - DX_3 x = E, \tag{14}$$

where $x = \begin{pmatrix} A_m \\ B_m \\ C_m \\ D_m \\ E_m \\ F_m \end{pmatrix}$, $X_j = \begin{pmatrix} 0 & 0 & 0 & 0 & 0 & 0 \\ 0 & X_m & 0 & 0 & 0 & 0 \\ 0 & 0 & 0 & 0 & 0 & 0 \\ 0 & 0 & 0 & X_m & 0 & 0 \\ 0 & 0 & 0 & 0 & 0 & 0 \\ 0 & 0 & 0 & 0 & 0 & X_m \end{pmatrix}$ with $j = 1$, $X_m = B_m$, $j = 2$, $X_m = D_m$, $j = 3$, $X_m = F_m$. The 6×6 matrix A is as follows:

$$A = \begin{pmatrix} 0 & 0 & 1 & T_1 & 2p_1 & 2T_1p_1 \\ 0 & 0 & 1 & T_2 & 2p_2 & 2T_2p_2 \\ 0 & 0 & 1 & T_3 & 2p_3 & 2T_3p_3 \\ 1 & T_1 & p_1 & T_1p_1 & p_1^2 & T_1p_1^2 \\ 1 & T_2 & p_2 & T_2p_2 & p_2^2 & T_2p_2^2 \\ 1 & T_3 & p_3 & T_3p_4 & p_3^2 & T_3p_3^2 \end{pmatrix}, \tag{15}$$

the matrix B is

$$B = \begin{pmatrix} 0 & \frac{T_1}{\rho_{m_1}^2 C_{p_{T_1}}} & 0 & \frac{2T_1}{\rho_{m_1}^2 C_{p_{T_1}}} p_1 & 0 & \frac{2T_1}{\rho_{m_1}^2 C_{p_{T_1}}} p_1^2 \\ 0 & \frac{T_2}{\rho_{m_2}^2 C_{p_{T_2}}} & 0 & \frac{2T_2}{\rho_{m_2}^2 C_{p_{T_2}}} p_2 & 0 & \frac{2T_2}{\rho_{m_2}^2 C_{p_{T_2}}} p_2^2 \\ 0 & \frac{T_3}{\rho_{m_3}^2 C_{p_{T_3}}} & 0 & \frac{2T_3}{\rho_{m_3}^2 C_{p_{T_3}}} p_3 & 0 & \frac{2T_3}{\rho_{m_3}^2 C_{p_{T_3}}} p_3^2 \\ 0 & 0 & 0 & 0 & 0 & 0 \\ 0 & 0 & 0 & 0 & 0 & 0 \\ 0 & 0 & 0 & 0 & 0 & 0 \end{pmatrix}, \tag{16}$$

the matrix C is

$$C = \begin{pmatrix} 0 & 0 & 0 & \frac{T_1}{\rho_{m_1}^2 C_{p_{T_1}}} p_1^2 & 0 & \frac{2T_1}{\rho_{m_1}^2 C_{p_{T_1}}} p_1^3 \\ 0 & 0 & 0 & \frac{T_2}{\rho_{m_2}^2 C_{p_{T_2}}} p_2^2 & 0 & \frac{2T_2}{\rho_{m_2}^2 C_{p_{T_2}}} p_2^3 \\ 0 & 0 & 0 & \frac{T_3}{\rho_{m_3}^2 C_{p_{T_3}}} p_3^2 & 0 & \frac{2T_3}{\rho_{m_3}^2 C_{p_{T_3}}} p_3^3 \\ 0 & 0 & 0 & 0 & 0 & 0 \\ 0 & 0 & 0 & 0 & 0 & 0 \\ 0 & 0 & 0 & 0 & 0 & 0 \end{pmatrix}, \tag{17}$$

the matrix D is

$$D = \begin{pmatrix} 0 & 0 & 0 & 0 & 0 & \frac{T_1}{\rho_{m_1}^2 C_{p_{T_1}}} p_1^4 \\ 0 & 0 & 0 & 0 & 0 & \frac{T_2}{\rho_{m_2}^2 C_{p_{T_2}}} p_2^4 \\ 0 & 0 & 0 & 0 & 0 & \frac{T_3}{\rho_{m_3}^2 C_{p_{T_3}}} p_3^4 \\ 0 & 0 & 0 & 0 & 0 & 0 \\ 0 & 0 & 0 & 0 & 0 & 0 \\ 0 & 0 & 0 & 0 & 0 & 0 \end{pmatrix}, \tag{18}$$

and $\mathrm{E}^t = \begin{pmatrix} \frac{1}{c_1^2} & \frac{1}{c_2^2} & \frac{1}{c_3^2} & \rho_{m_1} & \rho_{m_2} & \rho_{m_3} \end{pmatrix}$.

Eq. 14 can then be rearranged as follows:

$$\left(A - BX_1 - CX_2 - DX_3\right) x = E \Longleftrightarrow x = \left(A - BX_1 - CX_2 - DX_3\right)^{-1} E. \tag{19}$$

Noting that X_1, X_2, and X_3 are expressed as a function of x, Eq. 19 has the form $x = f(x)$, which can be solved efficiently by a fixed-point iteration method:

$$x_{j+1} = \left(A - BX_{1,i} - CX_{2,j} - DX_{3,j}\right)^{-1} E, \tag{20}$$

where j denotes the iteration level. The algorithm stops when $\left\| x_{j+1} - x_j \right\| \leq \varepsilon$, ε being a small real value.

Because the term $\frac{\alpha^2 T}{\rho C_p}$ in Eq. 11 is much smaller than κ_T, it is therefore possible to use

$$Ax_0 = E, \tag{21}$$

as an initial value for the fixed-point iteration method. In practice, the solution of Eq. 13 with the fixed-point iteration method does not require more than a half dozen iterations to achieve a stopping condition of $\varepsilon = 10^{-6}$.

Suppose the speed of sound can be measured with an uncertainty of 0.1 m/s and repeatability of 0.01 m/s, based, for example, on the characteristics of an inline combined densitometer and speed-of-sound sensor model L-Com 5500 from Anton Paar, then it is possible to proceed as before and estimate the range of pressures and temperatures required to obtain a predictability of the mass density over a range of 1000 bar and 200°C. The results in **Fig. 7** show that it is possible to achieve a precision better than 5% on average over the whole range of pressure and temperature of 1000 bar and 200°C, with three calibration measurements over a range of 60 bar and 5°C.

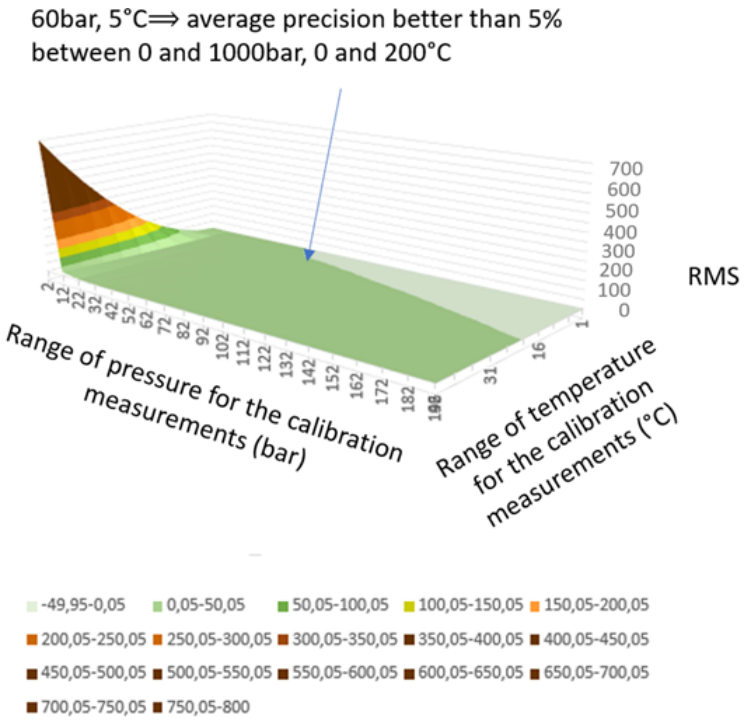

Fig. 7—RMS value of an extrapolated PVT model for a range of pressures spanning 1000 bar and a range of temperatures of 200°C, when the calibration measurements are taken within a range of temperatures given on the *x*-axis and a range of pressures given in the *y*-axis. The results are based on a densitometer having a measurement accuracy of 0.05 kg/m^3, a measurement of the speed of sound with an accuracy of 0.1 m/s, and 250 stochastic simulations.

This result shows that it is possible to reduce the number of pressure and temperature conditions to three by measuring the speed of sound in the drilling fluid in addition to the mass density. However, this reduction in the number of pressure and temperature conditions depends on knowing the specific heat of the drilling fluid, which is often not the case. In the next section, the influence of the fluid specific heat capacity on the heat transfer along an insulated pipe will be analyzed.

Heat Transfer along an Insulated Pipe after Passing a Heat Source

The definition of specific heat is (Landau and Lifshitz 1980) as follows:

$$C_p = \left(\frac{1}{m}\frac{\partial Q}{\partial T}\right)_p, \tag{22}$$

where Q is the amount of heat (i.e., it characterizes the amount of energy necessary to change the temperature of a given mass of matter).

The specific heat capacity of the drilling fluid can be obtained using a hydraulic circuit consisting of a pump, a volumetric flow-rate measurement, and an insulated pipe in which a drilling fluid is circulated with a heating element upstream of the pipe **(Fig. 8).**

Consider the energy conservation of a system under isobaric conditions (Corre et al. 1984):

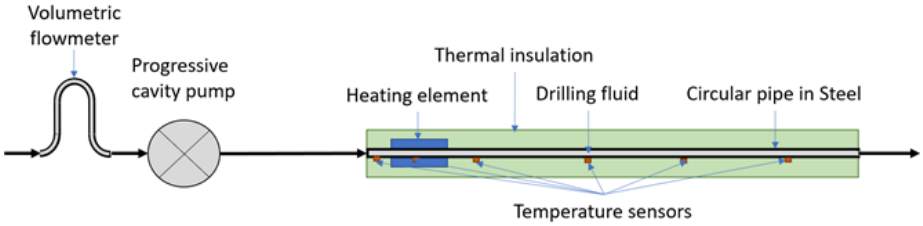

Fig. 8—Schematic view of a hydraulic circuit where drilling fluid flows inside a pipe that is thermally insulated and where there is a heat source that is positioned upstream of the pipe.

$$\frac{\partial \rho H}{\partial t} = \nabla \left(\vec{Q}_f + \vec{Q}_c \right) + q_s, \tag{23}$$

where H is the enthalpy per unit mass, $\vec{Q}_f = \rho_m H \vec{v}$ is the forced-convective heat flow, $\vec{Q}_c$ is the conductive and natural convective heat flow, and q_s is a heat source per unit time and per unit length.

For an isotropic solid, like steel or an insulating material, the pure conductive heat flow is expressed as follows:

$$\vec{Q}_c = \lambda \nabla T, \tag{24}$$

where λ is the thermal conductivity.

The Nusselt number in the heat flow direction (N_{uL}) is introduced to estimate the natural convective heat flow in a drilling fluid:

$$N_{u_L} = \frac{h_L L}{\lambda}, \tag{25}$$

where $h_L = \frac{q}{\Delta T}$ is the convective heat transfer coefficient in the heat flow direction, L is the characteristic length, q is the heat flux (i.e., thermal power per unit area), and ΔT is the temperature difference. For laminar flow, Corre et al. (1984) use the following expression of the Nusselt number (Corre et al. 1984):

$$N_{u_L} = -4 n_1 \ln \left(8 \psi \right), \tag{26}$$

where $n_1 = \frac{\pi \lambda_m L}{4 Q_v \rho_m C_{p_m}}$, Q_v is the volumetric flow rate, C_{pm} is the specific heat capacity of the drilling fluid, λ_m is the thermal conductivity of the drilling fluid, and ψ is defined as follows:

$$\psi \left(n_1 \right) = 0.10238 e^{-14.627 n_1} + 0.0122 e^{-89.22 n_1} + 0.00237 e^{-212 n_1}. \tag{27}$$

Furthermore, the convective wall heat flux in laminar flow conditions (q_w) is then (Barletta 1996)

$$q_w = \frac{\lambda N_{u_L}}{2 R_i} \left(T_w - T_m \right), \tag{28}$$

where R_i is the internal pipe radius, T_w is the wall temperature, and T_m is the drilling fluid temperature.

The enthalpy of a thermodynamic system is the sum of its internal energy U and the work required to achieve its pressure and volume:

$$H = U + pV. \tag{29}$$

In differential form, Eq. 29 can then be expressed as [see Landau and Lifshitz (1980) for a demonstration]:

$$dH = C_p dT + V \left(1 - \alpha T \right) dp. \tag{30}$$

Assuming that the pressure drop along the pipe length of **Fig. 8** is negligible, then $dH \approx C_p dT$, so the energy balance of the drilling fluid contained in the pipe can be expressed as:

$$\rho_m C_{p_m} \pi R_i^2 \frac{\partial T_m}{\partial t} = \rho_m C_{p_m} Q_v \frac{\partial T_m}{\partial s} + \pi \lambda_m N_{u_L} \left(T_i - T_m \right) + q_{s_{\Delta p}}, \tag{31}$$

where T_m is the drilling fluid temperature, s is the curvilinear abscissa, and T_i is the temperature of the wall inside the pipe. The characteristic length L of the Nusselt number is the internal pipe diameter (i.e., $L = 2R_i$). The hydraulic work arising from viscous pressure losses is

$$q_{s_{\Delta p}} = Q_v \Delta p. \tag{32}$$

The energy balance for the pipe and the insulation material is defined in a cylindrical coordinate system as

$$\rho_s C_{p_s} \frac{\partial T_s}{\partial t} = \lambda_s \left(\frac{\partial^2 T_s}{\partial s^2} + \frac{\partial^2 T_s}{\partial r^2} + \frac{1}{r} \frac{\partial T_s}{\partial r} \right) + q_{s_h}, \tag{33}$$

where ρ_s, C_{ps}, and λ_s are, respectively, the mass density, specific heat capacity, and thermal conductivity of the solid material of either the pipe or the insulation material, and q_{sh} is the generated heat per unit time and unit length of the heating element. Considering the axial symmetry of the system, the term $\frac{\partial^2 T_s}{\partial r^2}$ is necessarily equal to zero.

In steady-state conditions, without heat generation and in pure axial conduction, Eq. 33 can be written as follows:

$$\lambda_s \frac{\partial^2 T_s}{\partial s^2} = 0. \tag{34}$$

After integration over a cylindrical area between R_1 and R_2, the axial heat flux per unit length (q_a) is derived:

$$q_a = -\pi \left(R_2^2 - R_1^2\right) \lambda_s \frac{\partial T}{\partial s}. \tag{35}$$

The axial heat flux over an axial distance l can be estimated:

$$Q_a|_l = -\pi \left(R_2^2 - R_1^2\right) \lambda_s \frac{\Delta T_a}{l}, \tag{36}$$

where ΔT_a is the axial difference of temperature.

Similarly, in steady-state conditions without heat generation and in pure radial conduction, Eq. 33 can be written as follows:

$$\lambda_s \frac{1}{r} \frac{\partial T_s}{\partial r} = 0. \tag{37}$$

After integration over a shell of radius r and length l, the radial heat flux per unit radial distance (q_r) is as follows:

$$q_r = -2\pi r l \lambda_s \frac{\partial T}{\partial r}. \tag{38}$$

And therefore, the radial heat flux between R_1 and R_2 is

$$Q_r|_{R_1}^{R_2} = -2\pi l \lambda_s \frac{\Delta T_r}{\ln \frac{R_2}{R_1}}, \tag{39}$$

where ΔT_r is the radial temperature difference.

Analysis of the heat transfer along an insulated pipe after the fluid has passed a heat source shows that the temperature along the pipe depends not only on the specific heat capacity but also the thermal conductivity of the fluid.

Experimental Setup for Determining C_p and λ

Attaching temperature sensors to the outside of the pipe in **Fig. 8** enables the radial heat flux to be measured while circulating fluid in the system. This proposition was verified by constructing a flow loop similar to that shown in **Fig. 8**. **Fig. 9** shows a schematic view of the experimental setup. A 10-L tank is equipped with an agitator and copper coil through which tap water is circulated. The flow rate is controlled so that the temperature in the tank remains constant.

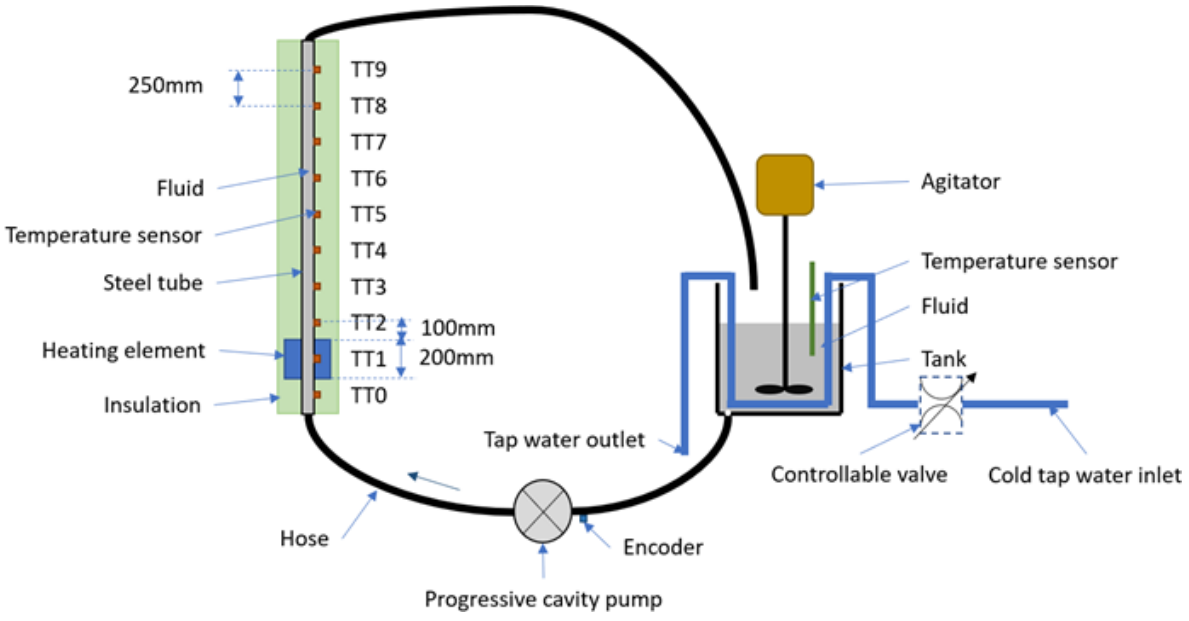

Fig. 9—Schematic representation of the experimental setup used to study the heat transfer along an insulated pipe.

A progressive cavity pump injects the fluid into the insulated instrumented pipe section. The pump is equipped with an encoder to measure the pump speed, and because there is very little pressure loss in the flow loop, the flow rate is directly proportional to the pump speed. The conversion factor from pump speed to volumetric flow rate has been calibrated by measuring the time to pump a known volume of fluid. The insulated pipe section comprises a 2-m length of 20-mm-diameter stainless-steel tube. Close to the inlet is a cylindrical aluminum block 200 mm in length and 100 mm in diameter heated by four resistors. A temperature sensor (TT1) is placed inside the aluminum block, and a controller regulates the electrical current to the heating resistor to regulate the temperature of the aluminum to a given set point. The remaining temperature sensors are placed 250 mm apart, and the insulation material is 30 mm thick.

Fig. 10 shows what happens when the heating element is turned on at 550 seconds, and then just after 3,100 seconds, when the flow rate is decreased from 0.451 to 0.096 L/min. The first temperature sensor downstream of the heating element (TT2 in **Fig. 10**) is positioned 100 mm above the top of the heating element and therefore is dominated by the heat conducted through the pipe with minimal influence from the circulating fluid. Because the mass density is known, temperature measurements at two different fluid velocities allow the specific heat capacity and the thermal conductivity of the drilling fluid **(Fig. 11)** to be derived from the heat transfer model described by Eqs. 31 and 33.

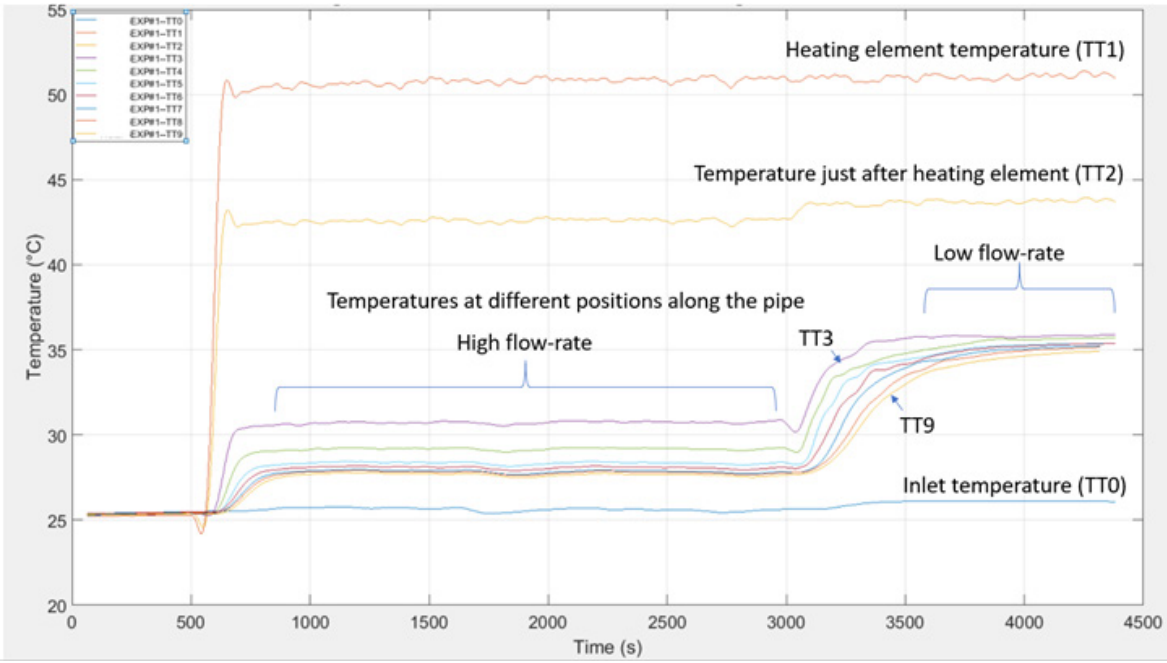

Fig. 10—In this experimental setup, there are 10 temperature sensors. The heating element is set to 50°C while circulating at 0.45 L/min at time 550 seconds. The flow rate is reduced to 0.1 L/min at time 3,100 seconds while the heating element is maintained at a constant temperature.

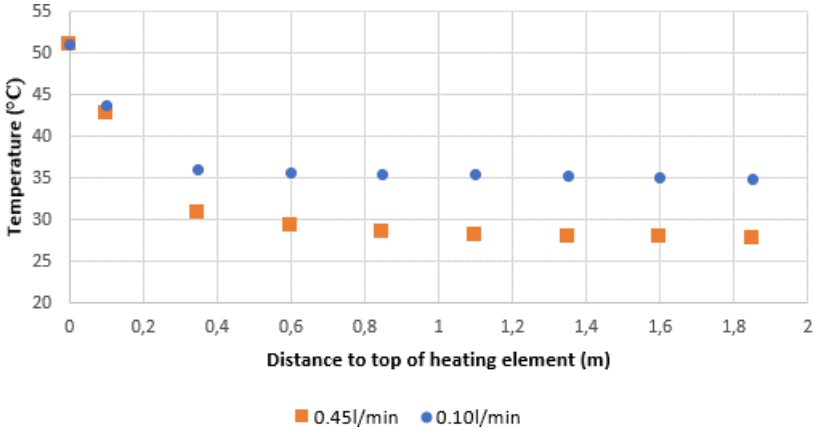

Fig. 11—Measured temperature above the top of the heating element for a flow rate of 0.45 and 0.10 L/min.

Overall Experimental Design

The measurement of radial heat flux along a pipe under varying flow conditions, shown in **Fig. 12,** with three stages of pressure and temperature permits the determination of the PVT properties of the fluid, as follows:

1. Ambient pressure and temperature conditions at the inlet
2. Increasing the temperature by 5–10°C at a pressure in the region of 50–60 bar
3. Increasing the temperature by a further 5–10°C with a pressure in the region of 25–30 bar

The volumetric flow rate and mass density at the inlet are measured with a Coriolis flowmeter. A speed-of-sound sensor is installed upstream of the inlet of the progressive cavity pump. In the second stage, a heating element downstream of the pump increases the fluid temperature by 5–10°C. A stainless-steel pipe is mounted on a thermal insulator downstream from the heating element. A differential pressure sensor measures the pressure losses along the pipe. The temperature distribution along a pipe is measured by at least four temperature sensors after which the mass density and speed of sound are again measured with a Coriolis flowmeter. The pressure in this

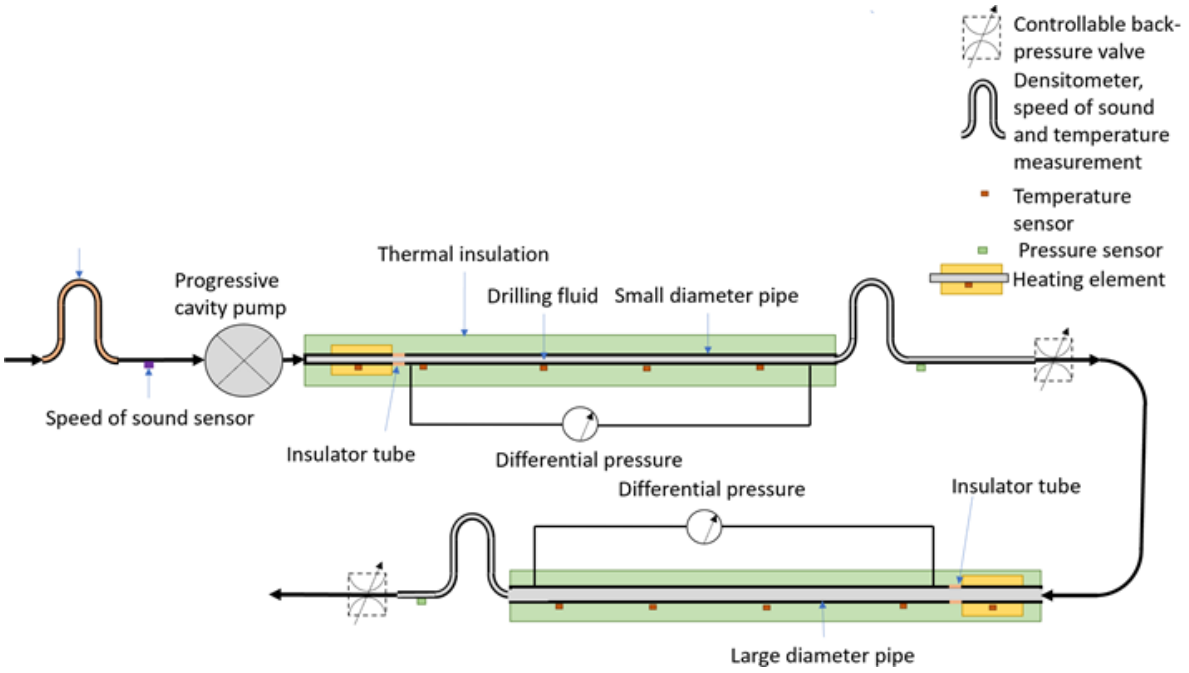

Fig. 12—Schematic representation of a setup that is capable of measuring the PVT behavior of a drilling fluid, its specific heat capacity, and thermal conductivity.

second stage is controlled by a choke downstream of the flowmeter. The third stage consists of a pipe of a different diameter from the first, designed to create flow conditions that differ from those in the previous stage. A similar heating element further increases the temperature. The pipe is thermally insulated from the heating element and, again, at least four temperature sensors are placed along the pipe to measure the temperature distribution as well as a differential pressure transducer. Another combined sensor measures the mass density and the speed of sound under the third set of conditions. The pressure in this third stage is controlled by a choke at the outlet.

The heat transfer (Eq. 31) depends on ρ_m, C_{pm}, λ_m, and the Nusselt number N_{uL}, which in turn depends on ρ_m, C_{pm}, λ_m. The solution of Eq. 31 gives the temperature evolution of the system. Because the fluid's mass density is measured, it remains to determine C_{pm} and λ_m. These parameters are obtained by solving the minimization problem:

$$\arg\min_{C_{pm},\lambda_m} \sum_{i=1}^{n_T} \left(T_i - \widetilde{T}_l \right)^2, \tag{40}$$

where T_i and $\widetilde{T}_l$ are, respectively, the measured and estimated temperatures at n_T different positions along the pipe. If Eq. 31 is divided by C_{pm}, then the equation depends on a term proportional to $\frac{\lambda_m N_{u_L}}{C_{p_m}}$ and $\frac{q_{s_{\Delta p}}}{C_{p_m}}$. Because the second term is small compared with the first, the temperature along the pipe is mostly influenced by the ratio of λ_m and C_{pm}. Because it is desired to explicitly determine the specific heat capacity of the fluid, it is necessary to create conditions that yield both the specific heat capacity and the thermal conductivity. Two dissimilar pipe sizes will result in different fluid velocities, allowing the term $\frac{q_{s_{\Delta p}}}{C_{p_m}}$ to elicit this difference.

Theoretical Model of Experimental Setup for Determining C_p and λ

To extract values of C_p and λ from the setup shown in **Fig. 12**, the system is discretized as shown in **Fig. 13** in n_a axial elements of length Δs (indexed by) and in radial elements of radial distance Δr (indexed by j). Similarly, time may be discretized in time steps of duration Δt (indexed by k).

Eq. 31 governs the heat transfer in the drilling fluid and in the air (outside of the system). For air, there are no heat sources, and there is no forced circulation; therefore, the energy balance at the external wall of the setup reduces to

$$\rho_{\text{air}} C_{p_{\text{air}}} \pi R_{n_r}^2 \frac{T_{i,n_r,k+1} - T_{i,n_r,k}}{\Delta t} = 2\pi R_{n_r} h_{\text{air}} \left(T_{\text{air}} - T_{i,n_r,k+1} \right), \tag{41}$$

where ρ_{air} is the mass density of air, $C_{p_{\text{air}}}$ is the specific heat capacity of air, R_{n_r} is the external radius, h_{air} is the air convective heat transfer coefficient, and T_{air} is the air temperature.

For the drilling fluid, heat generation arises from viscous pressure drops. Eq. 32 is used to estimate the heat generation caused by the passage of the fluid through the chokes. The energy balance at the internal wall of the pipe is

$$\rho_m C_{p_m} \pi R_1^2 \frac{T_{i,1,k+1} - T_{i,1,k}}{\Delta t} = \rho_m C_{p_m} Q_v \frac{T_{i+1,1,k+1} - T_{i,1,k+1}}{\Delta s} + \pi \lambda_m N_{u_L} \left(T_{i,1,k+1} - T_{m_i} \right) + Q_v \Delta p_i, \tag{42}$$

where R_1 is the internal radius of the pipe, T_{m_i} is the temperature of the fluid at axial position i, and Δp_i is the viscous pressure drop at axial position i. Note that Q_v and N_{u_L} also depend on the axial position.

For any other values of j, the energy conservation is based on Eq. 33:

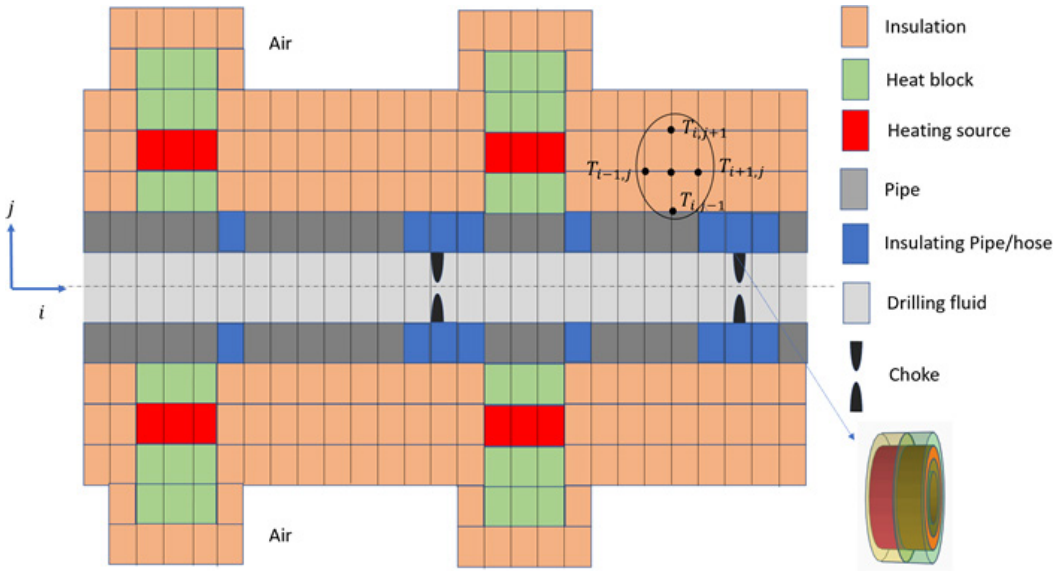

Fig. 13—Discretization of the setup for heat transfer calculations.

$$\rho_s C_{p_s}\pi\left(R^2_{j+\frac{1}{2}}-R^2_{j-\frac{1}{2}}\right)\frac{T_{i,j,k+1}-T_{i,j,k}}{\Delta t}=\pi\left(R^2_{j+\frac{1}{2}}-R^2_{j-\frac{1}{2}}\right)\rho_s\lambda_s\frac{T_{i,j,k+1}-T_{i+1,j,k+1}}{\Delta s}$$
$$+\pi\left(R^2_{j+\frac{1}{2}}-R^2_{j-\frac{1}{2}}\right)\rho_s\lambda_s\frac{T_{i-1,j,k+1}-T_{i,j,k+1}}{\Delta s}+2\pi\Delta s\lambda_s\frac{T_{i,j-1,k+1}-T_{i,j,k+1}}{\ln\frac{R_{j+\frac{1}{2}}}{R_{j-\frac{1}{2}}}}+2\pi\Delta s\lambda_s\frac{T_{i,j,k+1}-T_{i,j+1,k+1}}{\ln\frac{R_{j+\frac{1}{2}}}{R_{j-\frac{1}{2}}}}+q_{s_{h_i}}\quad,\tag{43}$$

where $R_{j+\frac{1}{2}}$ means the average radius between j and $j+1$ and $q_{s_{h_i}}$ is the heat generation at axial position i, if any.

After regrouping all the terms indexed $k+1$ on one side and the terms indexd k on the other, a system of linear equations is obtained. It can be solved for all $T_{i,j,k+1}$, for example, using a Gauss-Jordan method:

$$PT_{k+1}=R,\tag{44}$$

where P is a pentagonal matrix in which coefficients depend on the current boundary conditions and values estimated at the previous timestep k, T_{k+1} is a vector of unknown temperature at timestep $k+1$, and R is a vector of coefficients that depend only on the current boundary conditions and values estimated at the previous timestep k. The boundary conditions are the air temperature, the temperature of the pipe and the drilling fluid at the inlet, the volumetric flow rate at the inlet, the drilling fluid mass density in in-situ conditions, the specific heat capacity and the thermal conductivity of the drilling fluid, and the heat generated by the heating elements. In practice, a Crank-Nicolson scheme is used to improve the stability of the numerical resolution (Crank and Nicolson 1947). It is then possible to calculate, as a function of time, the temperature anywhere in the system and on the external side of the pipe.

Initial values of C_{p_m} and λ_m are unknown and therefore must be estimated. Because n_T temperatures are measured along the pipes, C_{p_m} and λ_m can be estimated by solving Eq. 40.

Setting $F=\sum_{l=1}^{n_T}\left(T_l-\widetilde{T}_l\right)^2=\sum_{l=1}^{n_T}r_l^2$, the sum of squared temperature differences, and defining $\beta^t=\begin{bmatrix}C_{p_m} & \lambda_m\end{bmatrix}$, the vector of model parameters. F is a minimum when

$$\forall j\in[1,2],\frac{\partial F}{\partial\beta_j}=\sum_{l=1}^{n_T}2r_l\frac{\partial r_l}{\partial\beta_j}=0.\tag{45}$$

Linearizing the solution vector from one iteration to another:

$$\beta_{\xi+1}=\beta_\xi+\Delta\beta,\tag{46}$$

where ξ is the iteration number. Then the first order approximation of $\widetilde{T}_l(\beta)$ is

$$\widetilde{T}_l(\beta)\approx\widetilde{T}_l(\beta_\xi)+\sum_{s=1}^{2}\frac{\partial\widetilde{T}_l(\beta_\xi)}{\partial\beta_s}(\beta_s-\beta_{s_\xi})=\widetilde{T}_l(\beta_\xi)+\sum_{s=1}^{2}J_{ls}\Delta\beta_s,\tag{47}$$

where $J_{ls} = \frac{\partial r_l}{\partial \beta_s}$ are the members of the Jacobian matrix J. Then, a first-order approximation of r_l is

$$r_l = T_l - \widetilde{T}_l(\beta) = T_l - \widetilde{T}_l(\beta_\xi) + \widetilde{T}_l(\beta_\xi) - \widetilde{T}_l(\beta) \approx \Delta T_{l,\xi} - \sum_{s=1}^{2} J_{ls}\Delta\beta_s, \tag{48}$$

where $\Delta T_{l,\xi} = T_l - \widetilde{T}_l(\beta_\xi)$ is the temperature difference for sensor l at iteration ξ. Substituting in Eq. 45, here is the resulting equation:

$$\forall j \in [1,2], \sum_{l=1}^{n_T} 2J_{lj}\left(\Delta T_{l,\xi} - \sum_{s=1}^{2} J_{ls}\Delta\beta_s\right) = 0, \tag{49}$$

which can be rewritten as follows:

$$\forall j \in [1,2], \sum_{l=1}^{n_T}\sum_{s=1}^{2} J_{lj}J_{ls}\Delta\beta_s = \sum_{l=1}^{n_T} J_{lj}\Delta T_{l,\xi}, \tag{50}$$

which is a system of linear equations that can be solved for $\Delta\beta$ resulting in a new value of β for the next iteration. The procedure stops when $\left\|\hat{\beta}\right\| \le \varepsilon$, where ε is small and $\hat{\beta}^t = \begin{bmatrix} \frac{C_{p_m}}{C_{p_0}} & \frac{\lambda_m}{\lambda_0} \end{bmatrix}$, which is a normalized version of the solution vector with C_{p_0} and λ_0 being chosen such that $\frac{C_{p_m}}{C_{p_0}}$ and $\frac{\lambda_m}{\lambda_0}$ are of the same order of magnitude for normal expected values of C_{p_m} and λ_m. When convergence is achieved, acceptable estimates of C_{p_m} and λ_m have been found. The Jacobian terms are estimated using a central difference approximation:

$$J_{ls} = \frac{\partial r_l}{\partial \beta_s} \approx \frac{r_l\left(\beta_s + \frac{\Delta h_s}{2}\right) - r_l\left(\beta_s - \frac{\Delta h_s}{2}\right)}{\Delta h_s}. \tag{51}$$

The initial values for $\beta_{\xi=0}$ are chosen from standard values for water/brines and base oils mixed with a quantity of barite that is necessary to obtain the current fluid mass density. Equations for determining the necessary amount of barite for a given mass density can be found in Cayeux (2020), and equations for estimating the specific heat capacity and thermal conductivity of a mix with solids can be found in Cayeux et al. (2014).

Having obtained values of C_p and λ, the parameters A, B, C, D, E, and F of the API PVT model can be calculated from Eq. 14.

Originally, only the specific heat capacity of the fluid (C_{p_m}) had to be determined to enable conversion of the isentropic to isothermal compressibility (Eq. 11). However, by designing a setup based on temperature measurements at different positions along a pipe downstream of a heat source, it was found that these temperatures depended not only on C_{p_m} but also on the fluid thermal conductivity (λ_m). While the determination of λ_m is a necessary step in establishing the value of C_{p_m} as a byproduct, it is a valuable input to additional downhole heat transfer calculations.

Discussion

An inline PVT measurement sensor for drilling fluids has been described. It reduces the number of pressure and temperature conditions required to predict the fluid densities by measuring the speed of sound in the medium. However, to obtain the isothermal compressibility of a drilling fluid, it is also necessary to measure its specific heat. Therefore, the initial design of the apparatus was modified to incorporate the measurement of temperatures along a pipe after applying a step change in temperature to the fluid. However, it has been found that the specific heat could not be determined without also finding another thermo-physical property of the fluid, namely, its thermal conductivity. An experimental setup was constructed to obtain these values, but, so far, the experiments have only been conducted with aqueous solutions of sodium chloride, potassium chloride brines, and methanol. After the initial experiments, it was found the design had to be modified based on the lessons learned from the first series of tests. It remains to be seen whether the new design based on constant flow rates with two pipe diameters provides the necessary measurement precision to calibrate the specific heat and thermal conductivity of the drilling fluid. In addition, the setup must be tested with both WBM and OBM. The precision of the apparatus over the wide range of pressures and temperatures depends on the availability of high-precision process industry densitometers and speed-of-sound sensors. Drilling fluids are notoriously difficult to analyze because of their high solids content. There is a risk of a deterioration in the accuracy of the sensors because of surface erosion of their internal pipes. This possibility will have to be tested in an experimental setup over extended periods to determine changes in accuracy against independent laboratory PVT measurements.

Future Work

The proposed design can provide the complete PVT behavior of the drilling fluid as well as its specific heat capacity and thermal conductivity continuously, in real time and without delay. The next step is to build a laboratory prototype of the proposed design to verify the working principle. The measured values will be compared with laboratory measurements of mass density made over a wide range of pressures and temperatures, as well as laboratory measurements of specific heat capacity and thermal conductivity. If the results are satisfactory then, after further refinement of the design, consideration will be given to the development of a system that can be used for field trials at the rigsite.

Conclusions

Knowledge of the PVT behavior of a drilling fluid is important for estimating downhole pressures during drilling operations. As the drilling fluid composition changes, it is difficult to define PVT behavior accurately based on sporadic mass density measurements made under ambient conditions at the surface.

A PVT model for a drilling fluid can be calibrated using a set of six pressure and temperature measurements. Calibration measurements made at low values of pressure and temperature can be reliably extrapolated to those to which the fluid is exposed when being circulated in the borehole, so long as the precision of the mass density measurement is in the order of 0.05 kg/m^3. However, a setup capable of measuring mass density under six different pressure and temperature conditions either would produce the PVT model parameters with substantial time delay if only one set of sensors is used or would require a relatively complex hydraulic setup to acquire the six sets of measurements simultaneously.

It has been shown that the number of pressure and temperature conditions can be reduced to three if the speed of sound in the drilling fluid is measured at the same time as the mass density. However, this method requires knowledge of the specific heat capacity of the drilling fluid. A method involving the addition of extra temperature sensors to the apparatus has been described. The additional temperature measurements are used to estimate the specific heat capacity of the fluid. The thermal conductivity of the fluid is also obtained as a valuable byproduct of the analytic procedure.

The outcome of this work is an inline setup that provides the PVT behavior of the drilling fluid as well as its specific heat capacity and thermal conductivity continuously and without delay. The latter two parameters are, of themselves, very important for heat transfer calculations in real-time model-predictive-control drilling automation applications.

Nomenclature

A = 6×6 matrix
A_m = parameter of the drilling fluid PVT model, ML^{-3}, kg/m^3
A_o = parameter of the oil-phase PVT model, ML^{-3}, kg/m^3
B = 6×6 matrix
B_m = parameter of the drilling fluid PVT model, $ML^{-3}\vartheta^{-1}$, kg/(m^{3}K)
B'_m = parameter of the drilling fluid PVT model, $ML^{-3}\vartheta^{-2}$, kg/(m^{3}K^2)
B_o = parameter of the oil-phase PVT model, $ML^{-3}\vartheta^{-1}$, kg/(m^{3}K)
B_w = parameter of the brine-phase PVT model, $ML^{-3}\vartheta^{-1}$, kg/(m^{3}K)
c = speed of sound, LT^{-1}, m/s
c_1 = speed of sound at conditions of pressure and temperature (p_1, T_1), LT^{-1}, m/s
c_2 = speed of sound at conditions of pressure and temperature (p_2, T_2), LT^{-1}, m/s
c_3 = speed of sound at conditions of pressure and temperature (p_3, T_3), LT^{-1}, m/s
C = 6×6 matrix
C_m = parameter of the drilling fluid PVT model, $L^{-2}T^{-2}$, kg/(m^{3}Pa)
C_o = parameter of the oil-phase PVT model, $L^{-2}T^{-2}$, kg/(m^{3}Pa)
C_p = isobaric specific heat capacity, $L^2T^{-2}\,\vartheta^{-1}$, J/(kg·K)
$C_{p_{\text{air}}}$ = specific heat capacity of air, $L^2T^{-2}\,\vartheta^{-1}$, J/(kg·K)
C_{p_m} = specific heat capacity of the drilling fluid, $L^2T^{-2}\,\vartheta^{-1}$, J/(kg·K)
C_{p_s} = specific heat capacity of a solid material, $L^2T^{-2}\,\vartheta^{-1}$, J/(kg·K)
C_w = parameter of the brine-phase PVT model, $L^{-2}T^{-2}$, kg/(m^{3}Pa)
D = 6×6 matrix
D_m = parameter of the drilling fluid PVT model, $L^{-2}T^{-2}\vartheta^{-1}$, kg/(m^{3}PaK)
D'_m = parameter of the drilling fluid PVT model, $L^{-2}T^{-2}\vartheta^{-2}$, kg/(m^{3}PaK^2)
D_o = parameter of the oil-phase PVT model, $L^{-2}T^{-2}\vartheta^{-1}$, kg/(m^{3}PaK)
D_w = parameter of the brine-phase PVT model, $L^{-2}T^{-2}\vartheta^{-1}$, kg/(m^{3}PaK)
E = 6×1 matrix
E_m = parameter of the drilling fluid PVT model, $L^{-1}M^{-1}T^{-4}$, kg/(m^{3}Pa^2)
E_o = parameter of the oil-phase PVT model, $L^{-1}M^{-1}T^{-4}$, kg/(m^{3}Pa^2)
E_w = parameter of the brine-phase PVT model, $L^{-1}M^{-1}T^{-4}$, kg/(m^{3}Pa^2)
f_i = volume fraction of the th component of the drilling fluid, dimensionless
F = sum of the square temperature differences, ϑ^2, K^2
F_m = parameter of the drilling fluid PVT model, $L^{-1}M^{-1}T^{-4}\vartheta^{-1}$, kg/(m^{3}Pa^{2}K)
F'_m = parameter of the drilling fluid PVT model, $L^{-1}M^{-1}T^{-4}\vartheta^{-2}$, kg/(m^{3}Pa^{2}K^2)
F_o = parameter of the oil-phase PVT model, $L^{-1}M^{-1}T^{-4}\vartheta^{-1}$, kg/(m^{3}Pa^{2}K)
F_w = parameter of the brine-phase PVT model, $L^{-1}M^{-1}T^{-4}\vartheta^{-1}$, kg/(m^{3}Pa^{2}K)
h_{air} = convective heat transfer coefficient, $MT^{-3}\vartheta^{-1}$, W/(m^{2}K)
h_L = convective heat transfer coefficient, $MT^{-3}\vartheta^{-1}$, W/(m^{2}K)
H = enthalpy per unit mass, L^2T^{-2}, J/kg
J = n_T×2 Jacobian matrix
l = length [L](m)
L = characteristic length, L, m
m = mass of drilling fluid contained in volume V, M, kg
n_a = number of axial elements
N_{u_L} = Nusselt number, dimensionless
p = absolute pressure, $ML^{-1}T^{-2}$, Pa
P = $n_a \cdot n_r \times n_a \cdot n_r$ matrix, $ML^2T^{-3}\vartheta^{-1}$,W/K
q = heat flux, MT^{-3}, W/m^2
q_a = axial heat flux per unit length, MLT^{-3}, W/m
q_r = radial heat flux per unit radial length, MLT^{-3}, W/m
q_s = heat source per unit time and per unit length, MLT^{-3}, W/m

q_{s_h} = heat source per unit time and per unit length generated by the heating element, MLT^{-3}, W/m
$q_{s_{\Delta p}}$ = heat source per unit time and per unit length generated by pressure loss, MLT^{-3}, W/m
q_w = convective wall heat flux in laminar conditions, MT^{-3}, W/m^2
Q = amount of heat, ML^2T^{-2}, J
$Q_a|_l$ = axial heat flux over a length l, ML^2T^{-3}, W
$\overrightarrow{Q_c}$ = conductive and natural convective heat flow, ML^2T^{-3}, W
$\overrightarrow{Q_f}$ = forced convective heat flow, ML^2T^{-3}, W
$Q_r|_{R_1}^{R_2}$ = radial heat flux between R_1 and R_2, ML^2T^{-3}, W
Q_v = volumetric flow rate, L^3T^{-1}, m^3/s
r = radial distance, L, m
r_l = difference of measured and estimated temperature at position l, ϑ, K
R = $n_a \cdot n_r$ vector, ML^2T^{-3}, W
R_1 = radial distance in a solid, L, m
R_2 = radial distance in a solid, L, m
R_i = internal pipe radius, L, m
s = curvilinear abscissa, L, m
S = entropy, $ML^2T^{-2}\,\vartheta^{-1}$, J/K
S_0 = parameter of the brine density model, ML^{-3}, kg/m^3
S_1 = parameter of the brine density model, ML^{-3}, kg/m^3
S_2 = parameter of the brine density model, ML^{-3}, kg/m^3
S_3 = parameter of the brine density model, ML^{-3}, kg/m^3
T = temperature, ϑ, K
T_{air} = air temperature, ϑ, K
T_i = temperature at the internal wall of the pipe, ϑ, K
T_l = measured temperature, ϑ, K
$\widetilde{T_l}$ = estimated temperature, ϑ, K
T_m = temperature of the drilling fluid, ϑ, K
T_{m_i} = drilling fluid temperature at axial position , ϑ, K
T_w = internal pipe wall temperature, ϑ, K
$\overrightarrow{v}$ = fluid velocity, LT^{-1}, m/s
w_t = weight fraction of a salt, dimensionless
x = 6×1 matrix
X_1 = 6×6 matrix
X_2 = 6×6 matrix
X_3 = 6×6 matrix
α = volumetric coefficient of thermal expansion, ϑ^{-1}, K^{-1}
α_{p_1,T_1} = volumetric coefficient of thermal expansion at conditions of pressure and temperature (p_1, T_1), ϑ^{-1}, K^{-1}
α_{p_2,T_2} = volumetric coefficient of thermal expansion at conditions of pressure and temperature (p_2, T_2), ϑ^{-1}, K^{-1}
α_{p_3,T_3} = volumetric coefficient of thermal expansion at conditions of pressure and temperature (p_3, T_3), ϑ^{-1}, K^{-1}
β = vector of the calibration parameters C_{p_m} and λ_m
$\hat{\beta}$ = vector of the normalized calibration parameters $\frac{C_{p_m}}{C_{p_0}}$ and $\frac{\lambda_m}{\lambda_0}$
Δp_i = viscous pressure drop at axial position , $ML^{-1}T^{-2}$, Pa
Δr = length of a radial element, L, m
Δs = length of an axial element, L, m
Δt = duration of a timestep, T, seconds
ΔT_a = axial temperature difference, ϑ, K
$\Delta T_{l,\xi}$ = difference between the l-temperature measurement and its corresponding estimated value at iteration ξ, ϑ, K
ΔT_r = radial temperature difference, ϑ, K
ε = small number, dimensionless
κ_{p_1,T_1} = isothermal compressibility coefficient at conditions of pressure and temperature (p_1, T_1), $M^{-1}LT^2$, Pa^{-1}
κ_{p_2,T_2} = isothermal compressibility coefficient at conditions of pressure and temperature (p_2, T_2), $M^{-1}LT^2$, Pa^{-1}
κ_{p_3,T_3} = isothermal compressibility coefficient at conditions of pressure and temperature (p_3, T_3), $M^{-1}LT^2$, Pa^{-1}
κ_S = isentropic compressibility, $M^{-1}LT^2$, Pa^{-1}
κ_T = isothermal compressibility coefficient, $M^{-1}LT^2$, Pa^{-1}
λ = thermal conductivity, $MLT^{-3}\vartheta^{-1}$, W/(m·K)
λ_m = thermal conductivity of the drilling fluid, $MLT^{-3}\vartheta^{-1}$, W/(m·K)
λ_s = thermal conductivity of a solid material, $MLT^{-3}\vartheta^{-1}$, W/(m·K)
ξ = iteration number in the calibration procedure for C_{p_m} and λ_m
ρ_{air} = mass density of air, ML^{-3}, kg/m^3
ρ_i = mass density of the component of the drilling fluid, ML^{-3}, kg/m^3
ρ_m = mass density of a drilling fluid, ML^{-3}, kg/m^3
ρ_{m_1} = mass density measurement at conditions of pressure and temperature (p_1, T_1), ML^{-3}, kg/m^3

ρ_{m_2} = mass density measurement at conditions of pressure and temperature (p_2, T_2), ML^{-3}, kg/m^3
ρ_{m_3} = mass density measurement at conditions of pressure and temperature (p_3, T_3), ML^{-3}, kg/m^3
ρ_{m_4} = mass density measurement at conditions of pressure and temperature (p_4, T_4), ML^{-3}, kg/m^3
ρ_{m_5} = mass density measurement at conditions of pressure and temperature (p_5, T_5), ML^{-3}, kg/m^3
ρ_{m_6} = mass density measurement at conditions of pressure and temperature (p_6, T_6), ML^{-3}, kg/m^3
ρ_s = mass density of a solid material, ML^{-3}, kg/m^3
ρ_w = mass density of a brine, ML^{-3}, kg/m^3
Ω = a set of indices for the components of the drilling fluid

Acknowledgments

Finally, I would like to extend a special thanks to John Thorogood for very fruitful discussions and valuable inputs during the preparation of this manuscript.

References

API RP 13D. 2017. *Recommended Practice on the Rheology and Hydraulics of Oil-Well Drilling Fluids*, fifth edition. Washington, DC: API.

Barletta, A. 1996. Fully Developed Laminar Forced Convection in Circular Ducts for Power-Law Fluids with Viscous Dissipation. *Int J Heat Mass Transf* **40** (1): 15–26. https://doi.org/10.1016/S0017-9310(96)00094-4.

Cayeux, E. 2020. *Mathematical Modelling of the Drilling Process for Real-Time Applications in Drilling Simulation, Interpretation and Assistance*. PhD Thesis, University of Stavanger, Stavanger, Norway.

Cayeux, E., Mesagan, T., Tanripada, S. et al. 2014. Real-Time Evaluation of Hole-Cleaning Conditions With a Transient Cuttings-Transport Model. *SPE Drill & Compl* **29** (1): 5–21. SPE-163492-PA. https://doi.org/10.2118/163492-PA.

Corre, B., Eymard, R., and Guenot, A. 1984. Numerical Computation of Temperature Distribution in a Wellbore While Drilling. Paper presented at the SPE Annual Technical Conference and Exhibition, Houston, Texas, USA, 16–19 September. SPE-13208-MS. https://doi.org/10.2118/13208-MS.

Crank, J. and Nicolson, P. 1947. A Practical Method for Numerical Evaluation of Solutions of Partial Differential Equations of the Heat Conduction Type. *Math Proc Camb Philos Soc* **43** (1): 50–67. https://doi.org/10.1017/S0305004100023197.

Demirdal, B. and Cunha, J. C. S. 2007. Olefin Based Synthetic Drilling Fluids' Volumetric Behavior Under Downhole Conditions. Paper presented at the Rocky Mountain Oil & Gas Technology Symposium, Denver, Colorado, USA, 16–18 April. SPE-108159-MS. https://doi.org/10.2118/108159-MS.

Demirdal, B. and Cunha, J. C. 2009. Olefin-Based Synthetic-Drilling-Fluids Volumetric Behavior Under Downhole Conditions. *SPE Drill & Compl* **24** (2): 239–248. SPE-108159-PA. https://doi.org/10.2118/108159-PA.

Demirdal, B., Miska, S., Takach, N. et al. 2007. Drilling Fluids Rheological and Volumetric Characterization Under Downhole Conditions. Paper presented at the Latin American & Caribbean Petroleum Engineering Conference, Buenos Aires, Argentina, 15–18 April. SPE-108111-MS. https://doi.org/10.2118/108111-MS.

Hemphill, T. and Isambourg, P. 2005. New Model Predicts Oil, Synthetic Mud Densities. *Oil Gas J* **103** (16): 56–58.

Hermoso, J., Martínez-Boza, F. J., and Gallegos, C. 2017. Organoclay Influence on High Pressure-High Temperature Volumetric Properties of Oil-Based Drilling Fluids. *J Pet Sci Eng* **151**: 13–23. https://www.sciencedirect.com/science/article/pii/S0920410517301742.

Hussein, A. M. and Amin, R. A. 2010. Density Measurement of Vegetable and Mineral Based Oil Used in Drilling Fluids. Paper presented at the Nigeria Annual International Conference and Exhibition, Tinapa - Calabar, Nigeria, 31 July–7 August. SPE-136974-MS. https://doi.org/10.2118/136974-MS.

Isambourg, P., Anfinsen, B. T., and Marken, C. 1996. Volumetric Behavior of Drilling Muds at High Pressure and High Temperature. Paper presented at the European Petroleum Conference, Milan, Italy, 22–24 October. SPE-36830-MS. https://doi.org/10.2118/36830-MS.

Kemp, N. P., Thomas, D. C., Atkinson, G. et al. 1989. Density Modeling for Brines as a Function of Composition, Temperature, and Pressure. *SPE Prod Eng* **4** (4): 394–400. SPE-16079-PA. https://doi.org/10.2118/16079-PA.

Landau, L. D. and Lifshitz, E. M. 1980. Course of Theoretical Physics. In *Statistical Physics*, Vol. 5. London, UK: Addison-Wesley.

McMordie, W. C., Bland, R. G., and Hauser, J. M. 1982. Effect of Temperature and Pressure on the Density of Drilling Fluids. Paper presented at the SPE Annual Technical Conference and Exhibition, New Orleans, Louisiana, USA, 26–29 September. SPE-11114-MS. https://doi.org/10.2118/11114-MS.

Peters, E. J., Chenevert, M. E., and Zhang, C. 1990. A Model for Predicting the Density of Oil-Based Muds at High Pressures and Temperatures. *SPE Drill Eng* **5** (2): 141–148. SPE-18036-PA. https://doi.org/10.2118/18036-PA.

Teukolsky, S. A., Flannery, B. P., Press, W. H. et al. 1992. *Numerical Recipes in C*. Cambridge, UK: Cambridge University Press.

Zamora, M., Broussard, P. N., and Stephens, M. P. 2000. The Top 10 Mud-Related Concerns in Deepwater Drilling Operations. Paper presented at the SPE International Petroleum Conference and Exhibition in Mexico, Villahermosa, Mexico, 1–3 February. SPE-59019-MS. https://doi.org/10.2118/59019-MS.

Zamora, M., Enriquez, F., Roy, S. et al. 2012. Measuring PVT Characteristics of Base Oils, Brines, and Drilling Fluids under Extreme Temperatures and Pressures. Paper presented at the AADE Fluids Technology Conference and Exhibition, Houston, Texas, USA, 10–11 April. AADE-12-FTCE-44.

Zamora, M., Roy, S., Slater, K. et al. 2013. Study on the Volumetric Behavior of Base Oils, Brines, and Drilling Fluids Under Extreme Temperatures and Pressures. *SPE Drill & Compl* **28** (3): 278–288. SPE-160029-PA. https://doi.org/10.2118/160029-PA.